Structural Control and Health Monitoring

Static structural system identification for beam-like structures using compatibility conditions

Journal:	*Structural Control and Health Monitoring*
Manuscript ID	STC-17-0022.R1
Wiley - Manuscript type:	Research Article
Date Submitted by the Author:	08-May-2017
Complete List of Authors:	Lei, Jun; Tongji University, Department of Bridge Engineering Xu, Dong; Tongji University, Department of Bridge Engineering Turmo, Jóse; Universitat Politecnica de Catalunya, Department of Civil and Environmental Engineering
Keywords:	beam-like, compatibility conditions, null space, static, observability, measurement errors, redundant set

Title: Static structural system identification for beam-like structures using compatibility conditions

Authors:

Name	Affiliation
Jun LEI,	Department of Bridge Engineering, Tongji University, Shanghai, China
Dong Xu	Department of Bridge Engineering, Tongji University, Shanghai, China
Jose Turmo	Department of Civil and Environmental Engineering, Universitat Politécnica de Catalunya BarcelonaTech, Barcelona, Catalunya, Spain

Corresponding Author:

Name: Dong XU

Title: Prof., Ph.D.

Address: Room 507, Department of Bridge Engineering, Tongji University,1239 Siping Road, Shanghai, China

Post: 200092

Email: xu_dong@tongji.edu.cn

Tel: 021-65980953

Fax: 021-65980953

Static structural system identification for beam-like structures using compatibility conditions

Abstract:

Due to the inevitable noise existing in the measured responses, Structural System Identification is often a challenging task in terms of the accuracy of the estimations. Structural System Identification by the observability method, which is characterized by the analysis of null spaces, is a powerful tool to determine the observability of structural parameters. However, it did not cope well with measurement errors so far. In this paper, for the first time, functional relations among displacements, denoted by the term compatibility conditions, in beam-like structures are derived by the observability method. Then compatibility conditions are imposed in an optimization procedure to minimize the discrepancy between the measured response and the compatible one. The compatible response obtained by the optimization is used to obtain the final estimations of the parameters. In a simply supported bridge example, the proposed method is thoroughly evaluated regarding the number of measurements, error levels and load cases. In an example of a continuous bridge, different load cases are used to estimate the bending stiffnesses of different zones. The accuracy and the efficacy of the proposed method are verified by the numerical results.

Keyword: static; observability; compatibility conditions; measurement errors; null space; redundant set; beam-like;

1.Introduction

Research interest in Structural System Identification (SSI) has been increasing over the years due to the strengthened computation power and the rapid development of various algorithms. Any SSI can be summarized as structural parameter estimation using discrete measurements of real-life structural response. A comprehensive description and the associated categories of SSI are provided in the technical report of ASCE[1]. These categories include static[2–7] and dynamic excitations[8–14], parametric[3,5] and non-parametric models[8,15–17], deterministic[2,4–6,9,18,19] and probabilistic approaches[10,20–24]. For both static and dynamic SSI methods, structural responses have to be measured to provide the necessary information. However, in dynamic methods, the knowledge of the mass and the damping is also required unless full sets of modes are known or the mass scaling factor can be determined by experimental means[14], which is not necessary for static SSI. In addition, dynamic methods require an adequate control of excitation including the elimination of spurious excitation which was essential for precise model-shape measurement, and the resolution of measurements for dynamic response was lower than that for static response[6]. In certain circumstances, static loading might be more economical than dynamic loading[5]. Hence, when only stiffness identification is required, static SSI might be more attractive than dynamic SSI. Based on the physical interpretability, SSI methods can be classified as parametric or non-parametric. In parametric methods, parameters correspond with the physical parameters (e.g. elastic moduli, areas, bending/torsional inertias), as they are used in finite element models (FEM). Non-parametric methods use basis functions to regress the response of the structure, e.g. autoregressive models[15,25] or rational fractional polynomials[16].

Concerning probabilistic SSI methods, mainly the Bayesian approach, posterior distributions of parameters are obtained by updating the assumed distributions of those parameters with the measured response. The estimations of the parameters can be obtained by point estimation (e.g. mean, median) or interval estimation (confidence interval) based on these posterior distributions. On the contrary, certainty is assumed for the parameters in deterministic SSI. Generally, deterministic methods try to pinpoint a unique solution of the problem. In both probabilistic and deterministic methods, optimization technique is closely involved. The objective of the optimization might be minimizing the discrepancy between the measured response and the predicted response,

e.g. displacements[4,5], strains[2,5], loads vector[5,6], acceleration[18], mode shapes and frequencies[9], or maximizing the sensitivity of the frequency response functions[19].

Observability Method (OM) is a mathematical tool dealing with the observability, i.e. the existence and the uniqueness, of the solution of a system of equations (or a subset of it)[26]. It has been applied to many engineering fields, e.g. water distribution systems[27], power systems[28], traffic networks[29]. An algebraic technique to analyze the observability of the solution of a linear system is checking the null space of the coefficient matrix[26]. This technique can be applied to the identification of parameters in physical and engineering problems in which the final systems are in the form of monomial ratio equations[30]. The application of OM has to be tailor-made due to the different characteristics of problems in different fields. The applicability of OM in SSI was verified in a cable-stayed bridge when investigating the measurement set to identify its mechanical properties[31]. At that time, the method was carried out in a symbolical approach to determine the observability of the parameters and estimations of those observable parameters were lacking. Later, a numerical development of this method was provided to determine the values of those observable parameters[4].

The observability problem in power system[28] considers a system with n parameters and m potential measurements. For the sake of economy and identifiability of the system, it is always desirable to know the least number of sensors required to identify these n parameters. In this context, the term essential sets relates to the measurement sets that ensure the identifiability of all n parameters while the drop of any measurement fails to do so. In the essential sets, the number of measurements is always the same as the number of parameters in the system. To address the issue of essential set in SSI by OM, observability tree method was proposed to analyze the identification sequence of the parameters[32]. It was shown that not all measurement sets could lead to global identifiability.

In SSI, there exist three sources of errors[33]: (1) Errors in measurements. (2) Errors in modeling. (3) Errors in parameter estimation. In most cases, measurement errors are assumed to follow the normal distribution with zero mean[6,34]. One way to mitigate the adverse effect of measurement errors is to use weight factors[5]. Each displacement was measured repeatedly and the variance in those measured values was calculated. Lower weight factors were assigned to displacements having high variances. This idea is similar to the weighted least square method[28]. Another way to deal with measurement errors is to implement SSI under a Bayesian probabilistic framework. In these methods, many sets of parameters are sampled from prior (assumed) distributions. For each set of sampled parameters, the posterior probability of obtaining the measured response with this parameter set being real is obtained. The final estimations of the parameters are determined by their posterior (updated) distributions using point or interval estimations. The main drawback of this method is that the intensity of the storage and the computation increase exponentially with the number of parameters. The effect of errors from measurements and parameter estimations was also investigated in SSI by OM for *essential sets*[35]. In the analytical expression of the identified bending stiffness, which is a quotient, it was found that measurement errors might render the sign of the denominator wrong. As a result, the estimations of the parameters might have no physical meaning and their variances are quite high. To deal with measurement errors, an intuitive idea is to measure more displacements. The term *redundant sets* is related with the case when redundant measurements are used in addition to *essential sets*[28]. These redundant measurements not only maintain the identifiability of the parameters in case of malfunction of sensors but also improve the accuracy of the estimations. However, using redundant measurements can be ineffective for SSI by OM because the denominator of the estimations might well be still close to zero or have a wrong sign. In order to fill this gap, the functional relations among the measured displacements, which are referred as the compatibility conditions, are derived algebraicaly in beam-like structures using OM for the first time. Then the incompatibility in measured displacements, which is caused by measurement errors, is reduced by an optimization routine with the compatibility conditions imposed. SSI is carried out using the compatible displacements eventually.

In the remaining part of this paper, section 2 introduces the general idea of SSI by OM. In section 3, the algorithm of SSI using compatibility conditions is proposed. Each step is detailed by the analysis on a simply supported beam bridge. In section 4, the accuracy of SSI by OM using redundant sets is provided first to emphasize the necessity of compatibility conditions. Then the performance of the proposed method is investigated regarding the effects of the number of measurements, error levels and load cases. In addition, the applicability of this method is verified by a continuous bridge example. Finally, some conclusions are drawn.

2.Structural System Identification by Observability Method

In SSI by OM[3], the FEM of the structure has to be defined first. Subsequently, the nodal equilibrium equations are obtained by direct analysis and then transformed into a system of monomial ratio equations. For illustration, assume that we have the following system of equations

$$K \cdot \delta = f \tag{1}$$

In Eq. (1), K, δ and f, respectively, represent the global stiffness matrix, the nodal displacements and the nodal forces. For 2D models with beam elements, the global stiffness matrix K is composed of the characteristics of the beam elements (i.e. length L, elastic moduli E, area A and inertia I). Displacement vector δ includes horizontal displacements u, vertical deflection v and rotation w whereas force vector f includes horizontal forces H, vertical forces V and moments M.

In direct analysis, every element in the matrix K and in the force vector f is assumed as known. The displacement vector δ is solved by Eq. (1). In SSI by OM, which is an inverse analysis, the matrix K is partially known. Parameters appearing in the matrix K are $\{E, A, I, L\}$. It is generally assumed that the length L is known while elastic moduli, E, areas, A, inertias, I are unknown. Since the main objective of SSI is to assess the condition of the structure, the estimations of axial stiffnesses EA and bending stiffnesses EI are of primary importance. To reduce unknowns, EA and EI, instead of being regarded as the product of two unknowns, are treated as one unknown each.

Once the unknowns in the matrix K, boundary conditions and measurements are determined, to solve Eq. (1) in a linearized form, it can be rearranged as:

$$K^* \cdot \delta^* = f \tag{2}$$

The operations to linearize Eq. (1) include: (1) the separation of the columns of matrix K, where some entries are the sum of different variables, into several single columns related with different variables, (2) the elimination of duplicated variables, (3) the merge of associated columns and (4) the extraction of the measured displacements from associated products and (5) the multiplication of them with the associated columns in the matrix K^*[3]. The modified matrix K^* has different dimensions from the matrix K. The linearized variables in the modified displacement vector δ^* might be non-linear products of the bending or axial stiffnesses and displacements, e.g. EAu, EIu, EIw and EIv, as well as single variables, e.g. EA, EI or nodal displacements. The variables in δ^* and f can be clustered into groups of known quantities, indicated by subscript 1, and unknown quantities, indicated by subscript 0, as shown in Eq. (3). δ_0^* includes variables associated with measured displacements or boundary conditions while δ_1^* includes variables containing the unknown displacements. Meanwhile, f_1 includes the external loads from the controlled static test while f_0 includes the reactions at the boundary conditions. The modified matrix K^* is partitioned accordingly.

$$\begin{pmatrix} K_{00}^* & K_{01}^* \\ K_{10}^* & K_{11}^* \end{pmatrix} \begin{Bmatrix} \delta_0^* \\ \delta_1^* \end{Bmatrix} = \begin{Bmatrix} f_0 \\ f_1 \end{Bmatrix} \tag{3}$$

In order to join the unknowns, Eq. (3) is transformed into Eq. (4).

$$B \cdot z = \begin{bmatrix} K_{10} & 0 \\ K_{00} & -I \end{bmatrix} \begin{Bmatrix} \delta_0^* \\ f_0 \end{Bmatrix} = \begin{Bmatrix} f_1 - K_{11}\delta_1^* \\ -K_{01}\delta_1^* \end{Bmatrix} = D \tag{4}$$

In Eq. (4), unknown variables are of two types: (1) Variables containing displacements (u, v or w), or stiffnesses (EA or EI), or the products of both, (EAu, EAv, EAw, EIu, EIv or EIw); or (2)

Reactions at the boundaries, *H, V* and *M*. The coefficient matrix *B* is composed of the measured displacements and the length of elements. Meanwhile, the right-hand side vector *D* is composed of the external loads f_1 and the equivalent nodal forces ($K_{11}\delta_1$ or $K_{01}\delta_1$). In short, the transformation from Eq. (3) to Eq. (4) collects all unknowns in *z*, and renders both *B* and *D* known.

As the observability of the solution of Eq. (4) are closely related with the concept of null space, its definition is given first. For a matrix $\mathcal{P}$, its null space is the vector space whose vectors *v* always satisfy Eq. (5).

$$\mathcal{P} \cdot v = 0 \tag{5}$$

From linear algebra, vector *v* is always a linear combination of basis vectors of the null space of the matrix $\mathcal{P}$. Then the null space matrix *N* is defined as the matrix whose columns are these basis vectors, this is to say, the columns of the null space matrix *N* form the basis of the null space. For Eq. (4) to have a solution, it is sufficient to check that the product of the transpose of the right-hand side vector, D^T, and the null space matrix N^* of the transpose of the matrix *B*, is a null (zero) vector, i.e. $D^T \cdot N^* = 0$. If this holds, the solution of Eq. (4) has the structure:

$$z_g = z_p + z_h = \begin{Bmatrix} \delta_0^* \\ f_0 \end{Bmatrix}_p + N \cdot \rho \tag{6}$$

where z_p is a particular solution of Eq. (4). It can be obtained by Moore-Penrose pseudoinverse or least squares methods. z_h is a vector from the null space of matrix *B*, which is a linear combination of basis vectors of this null space. The columns of the null space matrix *N* correspond with these basis vectors while the vector ρ is composed of the coefficients of the linear combination.

Furthermore, null rows in the matrix *N* render associated elements of $N \cdot \rho$ null. As a result, in the general solution, the variables related to these null rows are equal to their values in the particular solution. In this case, these variables are determined and unique, i.e. observable. This is to say, the inspection of the matrix *N* and the identification of its null rows lead to the identification of the observable variables. When the product of the transpose of the right-hand side vector, D^T, and the null space matrix N^* of the transpose of the matrix *B*, is not null , i.e. $D^T \cdot N^* \neq 0$, then Eq. (4) is not compatible and no solution exists[26].

When the observability of unknown variables is determined, the values of those observable variables are determined by the particular solution z_p of Eq. (4). It is to highlight that in SSI by OM, if any deflection, force or structural parameter is observed, this information might help to observe new parameters in the adjacent beam elements through a recursive process. In this analysis, the observed information is successively introduced as new input data in the observability analysis. The peculiarity of this method is illustrated by a detailed step-by-step example in previous studies[3,31].

3. SSI for beam-like structures using compatibility conditions

Measurement errors always arise in real life due to uncontrollable factors, e.g. the change in temperature, ambient vibration due to wind. Measured displacements might not be compatible due to these errors. In this section, in order to smooth away the incompatibility among measured displacements, SSI for beam-like structures using compatibility conditions is proposed. The derivation of compatibility conditions among displacements and the procedures for incorporating these conditions into an optimization are illustrated by a simply supported bridge example. A summary of the proposed method is presented at the end.

3.1 Example 1

In this section, a simply supported bridge is analyzed. The nine steps required to carry out SSI for beam-like structures using compatibility conditions are exemplified by this structure.

Multi-span simply supported bridges (Figure 1.a) are one of the most popular bridge types in practice. Example 1 (Figures 1.b) corresponds with an 18 m span of this arrangement. The cross

section of the structure is constant and the bending stiffness is 2.3×10^9N·m^2. A 350kN vertical load is applied at one-third point of the span. In this example, the targeted parameters are the bending stiffnesses, since the axial behavior is not activated by this load case.

Step 1: Introduce the geometry, as well as the known mechanical and geometrical properties and measured node forces to establish a FEM for the beam-like structure.

The FEM associated with Example 1 is shown in Figure 1.c. It is composed of 18 one-meter long elements. The bending stiffnesses for elements 1~6, 7~12 and 13~18 are assumed as EI_1, EI_2 and EI_3, respectively. Their real values are 2.3×10^9N·m^2, i.e. $EI_{1,r}=EI_{2,r}=EI_{3,r}=2.3\times10^9$N·m^2. An external load is applied at node 7, i.e. V_7=-350kN.

Step 2: Choose three nodal displacements belonging to elements with the same structural parameter and build Eq. (4) using these displacements.

Relations among nodal displacements that belong to the elements of the same bending stiffness can be found using OM. For instance, some relations among v_7~v_{13} and w_7~w_{13} exist since elements 7 to 12 have the same bending stiffness EI_2. Without loss of generality, the derivation of these relations is exemplified by the measurement set $\{w_7, v_{10}, w_{13}\}$. It is to highlight that a different set (e.g. $\{v_7, w_8, v_{11}\}$ or $\{v_9, v_{12}, v_{13}\}$) does not affect the result. The general equations (Eq. (4)) corresponding with this FEM and $\{w_7, v_{10}, w_{13}\}$ is obtained first (not shown here for the sake of brevity). In this equation, the coefficient matrix, the unknown vector and the right-hand side vector are denoted by B_1, z_1 and D_1, respectively.

Step 3: Check the null space matrix N of coefficient matrix B of Eq. (4) to obtain the observable unknowns.

The null space matrix N_1 of the coefficient matrix B_1 is provided in Eq. (7).

$$N_1 = \begin{pmatrix} 1/w_7 & 0 & \cdots & EI_1 \\ 1 & 0 & \cdots & EI_1v_2 \\ 2 & 0 & \cdots & EI_1v_3 \\ 3 & 0 & \cdots & EI_1v_4 \\ 4 & 0 & \cdots & EI_1v_5 \\ 5 & 0 & \cdots & EI_1v_6 \\ 6 & 0 & \cdots & EI_1v_7 \\ 1 & 0 & \cdots & EI_1w_1 \\ 1 & 0 & \cdots & EI_1w_2 \\ 1 & 0 & \cdots & EI_1w_3 \\ 1 & 0 & \cdots & EI_1w_4 \\ 1 & 0 & \cdots & EI_1w_5 \\ 1 & 0 & \cdots & EI_1w_6 \\ 0 & 0 & \cdots & EI_2 \\ 0 & 0 & \cdots & EI_2v_7 \\ 0 & 0 & \cdots & EI_2v_8 \\ 0 & 0 & \cdots & EI_2v_9 \\ 0 & 0 & \cdots & EI_2v_{11} \\ 0 & 0 & \cdots & EI_2v_{12} \\ 0 & 0 & \cdots & EI_2v_{13} \\ 0 & 0 & \cdots & EI_2w_8 \\ 0 & 0 & \cdots & EI_2w_9 \\ 0 & 0 & \cdots & EI_2w_{10} \\ 0 & 0 & \cdots & EI_2w_{11} \\ 0 & 0 & \cdots & EI_2w_{12} \\ . & . & \cdots & . \\ . & . & \cdots & . \\ . & . & \cdots & . \\ 0 & 0 & \cdots & V_1 \\ 0 & 0 & \cdots & V_{19} \end{pmatrix} \quad (7)$$

It is seen that all the rows related with EI_2, EI_2v_7~EI_2v_{13} and EI_2w_8~EI_2w_{12} are zeros. Hence, EI_2, EI_2v_7~EI_2v_{13} and EI_2w_8~EI_2w_{12} are observable. Also, reactions, V_1 and V_{19} are observable since this is a statically determinate structure. However, for any row related with EI_1 or associated products (e.g. EI_1v_2, EI_1w_1), at least one element of that row is nonzero. Hence, these unknowns are not observable. Specifically, due to insufficient information of the displacements of nodes 1~7, the first column of N_1 implies a rigid body motion of rotation. This is, the rotations indicated by EI_1w_1~EI_1w_6 are the same while the deflections of these nodes can be calculated by the product of this rotation and the distance between the current node and node 1.

Step 4: Derive the compatibility conditions and analytical expression for the i^{th} structural parameter from those observable unknowns.

Once the observable unknowns are detected, their estimations are specified by the associated values of the particular solution. For instance, the particular solutions for EI_2 and EI_2v_7 are provided in Eqs. (8) and (9).

$$\widehat{EI_2} = \frac{18V_7L}{\frac{(w_7 - w_{13})}{L}} \tag{8}$$

$$\widehat{EI_2v_7} = -\frac{3V_7L^3(25w_7 - 12v_{10} + 11w_{13})}{2(w_7 - w_{13})} \tag{9}$$

The hat, ^, denotes an estimation of the unknown. The physical meaning of the analytical expression of EI_2, Eq. (8), can be interpreted as the quotient of a moment expressed by the product of force and length and a curvature expressed by the displacements within elements of EI_2.

Rearranging the quotient between Eqs. (9) and (8) leads to the compatibility condition among $\{v_7, v_{10}, w_7, w_{13}\}$, as presented in Eq. (10)

$$12v_7 - 12v_{10} + 25w_7 + 11w_{13} = 0 \tag{10}$$

The compatibility conditions linking $\{w_7, v_{10}$ and $w_{13}\}$ and each of $\{v_7$~v_{13} and w_8~$w_{12}\}$ are found in the same way for elements of EI_2. It should be pointed out that regardless of the selected measurement set, the derivation of compatibility conditions always leads to identical mathematical equations.

Step 5: Repeat steps 2~4, until compatibility conditions and analytical expressions have been obtained for all parameters

Similarly, compatibility conditions among $\{v_2$~v_7, w_1~$w_7\}$ for EI_1 and those among $\{v_{13}$~v_{18}, w_{13}~$w_{19}\}$ for EI_2 as well as the analytical expressions for EI_1 and EI_2 are obtained.

It is pointed out that for one given bending stiffness, the functional relations among the nodal displacements belonging to elements with this stiffness are obtained by the repetition of steps 2~4.

Step 6: Form an underdetermined system by combining all compatibility conditions

It is seen that displacements for beam elements with the same stiffness (EI_1, EI_2 or EI_3) are dependent on three displacements within these elements (being aware that boundary conditions can reduce this number). In a more general case, a set of 7(=2+3+2) adequate displacements is needed to specify every displacement in this structure. Assume $\{w_1, w_3\}$, $\{w_8, v_9, w_{11}\}$ and $\{w_{15}, w_{19}\}$ are chosen for EI_1~EI_3, respectively. Note that the displacements of joint nodes for elements with different parameters, e.g. v_7 for EI_1 and EI_2, determined by different compatibility conditions should be equal to each other. Hence, 4 more equations can be imposed, i.e. $v_7(w_1, w_3) = v_7(w_8, v_9, w_{11})$, $w_7(w_1, w_3) = w_7(w_8, w_{11})$, $v_{13}(w_8, v_9, w_{11}) = v_{13}(w_{15}, w_{19})$ and $w_{13}(w_8, w_{11}) = w_{13}(w_{15}, w_{19})$. This forms an underdetermined system with 4 equations and 7 unknowns ($\{w_1, w_3, w_8, v_9, w_{11}, w_{15}$ and $w_{19}\}$). Hence, 3 out of the 7 adequate displacements are independent due to the 4 additional equations.

It is pointed out that all the compatibility conditions are related together by the displacements of those joint nodes between elements with different stiffnesses. From the resulting underdetermined system, a set of independent displacements can be obtained

Step 7: Choose a set of independent displacements in Step 6 as a condensed set $\hat{\boldsymbol{\delta}}_c$. Express all compatible displacements $\hat{\boldsymbol{\delta}}$ and structural parameters $\boldsymbol{\theta}$ as functions of $\hat{\boldsymbol{\delta}}_c$. That is, derive the functional relations $\hat{\boldsymbol{\delta}}_i = \boldsymbol{f}_i(\hat{\boldsymbol{\delta}}_c)$ and $\boldsymbol{\theta}_j = \boldsymbol{g}_j(\hat{\boldsymbol{\delta}}_c)$.

After steps 5 and 6, the relations among the nodal displacements belonging to elements with same stiffnesses as well as those associated with different stiffnesses are obtained. The displacements satisfy all these relations are referred as the compatible ones, $\hat{\delta}$. Note that all these displacements $\hat{\delta}$ are functions of a condensed set $\hat{\delta}_c$ (the independent displacements obtained in step 6). Specifically, $f_i(\hat{\delta}_c)$ is the functional form of the i^{th} compatible displacement $\hat{\delta}_i$ while $g_j(\hat{\delta}_c)$ is the functional form of the j^{th} parameter θ_j.

Without loss of generality, $\hat{\delta}_c$ is selected as $\{w_1, v_9 \text{ and } w_{19}\}$ since three displacements among $\{w_1, w_3, w_8, v_9, w_{11}, w_{15} \text{ and } w_{19}\}$ are independent (step 6). In this case, the functional relations $f_i(\hat{\delta}_c)$ for $\{w_3, w_8, w_{11} \text{ and } w_{15}\}$ are presented in Eqs. (11)~(14).

$$w_3 = 2(54v_9 + 1189w_1L + 17w_{19}L)/3123L \tag{11}$$

$$w_8 = -(2356w_1L - 519v_9 + 280w_{19}L)/2776L \tag{12}$$

$$w_{11} = -2(21v_9 + 19w_1L + 103w_{19}L)/(347L) \tag{13}$$

$$w_{15} = (352w_1L - 378v_9 + 575w_{19}L)/3123L \tag{14}$$

Regarding the functional form for bending stiffness, for instance, $\widehat{EI}_2$ can be determined by w_7 and w_{13} from Eq. (8). As these two rotations are functions of $\hat{\delta}_c$, the functional form for $\widehat{EI}_2$ in terms of $\hat{\delta}_c$ is also available.

Step 8: Find the optimal $\hat{\boldsymbol{\delta}}_c$ by minimizing the square sum of the proportional deviation of the compatible displacements, $\hat{\boldsymbol{\delta}}$, from the measured displacements, $\tilde{\boldsymbol{\delta}}$, as indicated by Eq. (15).

To smooth away the incompatibility in the measured displacements, the square sum of the proportional deviation of the i^{th} compatible displacement, $\hat{\delta}_i$, from the i^{th} measured displacement, $\tilde{\delta}_i$, is minimized, as indicated by Eq. (15).

$$F(\hat{\delta}_c) = \sum_{i=1}^{N_m} \left(\frac{\hat{\delta}_i}{\tilde{\delta}_i} - 1 \right)^2 = \sum_{i=1}^{N_m} \left(\frac{f_i(\hat{\delta}_c)}{\tilde{\delta}_i} - 1 \right)^2 \tag{15}$$

in which N_m is the number of measured displacements.

Step 9: Evaluate the structural parameters by providing the optimal $\hat{\boldsymbol{\delta}}_c$ to SSI by OM.

The best estimations of the bending stiffnesses are determined by providing the optimal $\hat{\delta}_c$ to SSI by OM.

3.2 Algorithm for SSI using compatibility conditions

All the necessary procedures to implement SSI for beam-like structures using compatibility conditions are presented in Figure 2 and summarized as follows.

Step 1: Introduce the geometry, as well as the known mechanical and geometrical properties and measured node forces to establish a FEM for the beam-like structure.

Step 2: Choose three nodal displacements belonging to elements with the same structural parameter and build Eq. (4) using these displacements.

Step 3: Check the null space matrix N of coefficient matrix B of Eq. (4) to obtain the observable unknowns.

Step 4: Derive the compatibility conditions and analytical expression for the i^{th} structural parameter from those observable unknowns.

Step 5: Repeat steps 2~4, until compatibility conditions and analytical expressions have been obtained for all parameters

Step 6: Form an underdetermined system by combining all compatibility conditions

Step 7: Choose a set of independent displacements in Step 6 as a condensed set $\hat{\delta}_c$. Express all compatible displacements $\hat{\delta}$ and structural parameters θ as functions of $\hat{\delta}_c$. That is, derive the functional relations $\hat{\delta}_i = f_i(\hat{\delta}_c)$ and $\theta_j = g_j(\hat{\delta}_c)$.

Step 8: Find the optimal $\hat{\delta}_c$ by minimizing the square sum of the proportional deviation of the compatible displacements, $\hat{\delta}$, from the measured displacements, $\tilde{\delta}$, as indicated by Eq. (15).

Step 9: Evaluate the structural parameters by providing the optimal $\hat{\delta}_c$ to SSI by OM.

4. Application of the compatibility conditions

In this section, the accuracy of SSI by OM using redundant measurements without imposing compatibility conditions is presented first. Then the performance of the proposed method is investigated in a simply supported beam with respect to the number of measurements, N_m, error levels, E_{level}, and load cases. At the end of this section, the applicability of this method is verified in a continuous beam.

4.1 Example 1 without compatibility conditions

The redundant set $\{v_3, v_5, v_7, v_9, v_{11}, v_{13}, v_{15}, v_{17}\}$($N_m$=8) is studied first. The measured displacements, $\tilde{\delta}$, are simulated by adding proportional noise to the real displacements, δ_r, as presented in Eq. (16). This proportional noise is the product of a specified error level, E_{level}, and a random number, χ. This random number χ follows a normal distribution with zero mean and standard deviation of 0.5, and it is truncated by the interval [-1,1].

$$\tilde{\delta} = \delta_r \cdot (1 + E_{level} \cdot \chi), \quad (16)$$

2000 numerical simulations of the identification of bending stiffnesses using error levels from 1% to 8% were carried out without imposing compatibility conditions[4]. As the number of equations exceeds the number of unknowns, the ill-posed problem was solved using the Penrose inverse subroutine provided by Matlab. To normalize the estimations, all the estimations are divided by their real values, which are denoted by a hat and the subscript r, i.e. $\hat{}_r$. This normalization is followed in the rest of the paper. Unless otherwise stated, estimations always refer to those normalized ones.

Without imposing some restrictions to the estimations, the method is useless due to the existence of extreme values[35]. Thus, the average is taken for those estimations falling into the range of [0.5, 1.5]. Table 1 presents the mean of the estimations of associated parameters under different error levels using 8 measurements.

From this table, it can be concluded that, when compatibility conditions are not imposed: (1) Regardless of the error level, great bias exists despite redundant measurements are used; (2) The bias is sensitive to the error levels; (3) Using redundant measurements fails to improve the accuracy of the estimation via SSI by OM.

4.2 Example 1 with compatibility conditions: Effect of the number of measurements

To investigate the effect of the number of measurements, three measurement sets are studied here. Apart from the set N_m=8 in section 4.1, the other two sets are $\{v_3 \sim v_5, v_7, v_9 \sim v_{11}, v_{13}, v_{15} \sim v_{17}\}$ (N_m=11) and $\{v_2 \sim v_{18}\}$ (N_m=17). Note that the locations of measurements in both sets, set N_m=8 and set N_m=11,

are included in the locations of measurements in set N_m=17. 2000 samples of measured displacements associated with set N_m=17 are generated with an error level of 4%. Then the samples for sets N_m=8 and N_m=11 are generated by taking the corresponding measurements in set N_m=17.

Figure 3 compares the accuracy of the estimations using these three sets. The accuracy of the proposed method is evaluated by the mean of the estimations while the robustness and confidence of the method are evaluated by the coefficient of variation (COV) in the estimations. Small COV of the estimations indicates a low dispersion.

In Figures 3.a and 3.b, it is seen that 8 measurements are sufficient to estimate $\widehat{EI}_{1,r}$ and $\widehat{EI}_{2,r}$ accurately with a low dispersion of the estimations. In the case of $\widehat{EI}_{3,r}$, a slight overestimation of 1.3% is observed, which is acceptable. However, the COV of the estimations in $\widehat{EI}_{3,r}$ is 0.112, which might not be negligible. When the number of measurements increases, the mean and the COVs of the estimations of the stiffnesses get closer to one and decrease, respectively. In addition, the improvement in $\widehat{EI}_{3,r}$ is relatively large when compared with the improvements in $\widehat{EI}_{1,r}$ and $\widehat{EI}_{2,r}$. In Figure 3.b, the drop of COV for $\widehat{EI}_{3,r}$ is roughly twice the drop of COV in $\widehat{EI}_{1,r}$ and $\widehat{EI}_{2,r}$ when the number of measurements increases. However, despite the fact that using more measurements reduces the extent of dispersion, the COV of the estimations of $\widehat{EI}_{3,r}$ using 17 measurements is still higher than the COV of the estimations of $\widehat{EI}_{1,r}$ or $\widehat{EI}_{2,r}$ using 8 measurements. The improvements of the results can be noticed when compared with those in Table 1, where for 8 measurements and a 4% error the results were far from acceptable. The worse accuracy observed in $\widehat{EI}_{3,r}$ compared with those results of $\widehat{EI}_{1,r}$ and $\widehat{EI}_{2,r}$ are in accordance with a previous study[35]. In fact, for a given load test, the lowest the curvature in a given area of the structure, the worst the accuracy of the estimated parameters in that zone.

The analysis of the effect of the number of measurements shows that: (1) For zones where curvature is excited, small number of measurements is sufficient to achieve reasonable accuracy. (2) The more the measurements, the less the deviation and the dispersion of the estimations. (3) Greater improvement in the accuracy of the estimations is seen for parameters in low curvature zones than those in high curvature zones. (4) The curvature level is more important than the number of measurements.

4.3 Example 1 with compatibility conditions: Effect of error levels

The effect of error levels is investigated here using the set N_m=8. The studied error levels range from 1% to 8%. For each error level, 2000 samples are generated by Eq. (16). The mean and COV of the estimations under different error levels are summarized in Figure 4. In Figure 4.a, the mean of the estimations increases slightly with the error level. However, the sensitivity of the structural parameters to the error levels is quite different. When E_{level} increases from 1% to 8%, the changes in the mean of $\widehat{EI}_{2,r}$ and $\widehat{EI}_{1,r}$ are 1.06% and 1.96% respectively, which are negligible. However, in the case of $\widehat{EI}_{3,r}$, the associated change is 5.26%, which is comparatively large. The order of sensitivity to error levels for these parameters is $\widehat{EI}_{3,r} > \widehat{EI}_{1,r} > \widehat{EI}_{2,r}$. In addition, overestimation can be observed for all parameters. The extent of the overestimation follows the same order. In Figure 4.b, COV for all parameters grows linearly with the error levels. Again, the COV of $\widehat{EI}_{3,r}$ is much higher than those of $\widehat{EI}_{1,r}$ and $\widehat{EI}_{2,r}$.

Hence, it can be concluded that: (1) For zones where curvature is excited, the deviation in the mean of the estimation is not sensitive to the error levels; (2) The level of dispersion (COV) increases linearly with the error levels; (3) The increase of deviation and dispersion is much faster in low curvature zones.

4.4 Example 1 with compatibility conditions: Effect of load cases

In section 4.2 and 4.3, slight overestimation and large dispersion are observed in low curvature zones. To investigate the influence of curvature, the external load is moved from the left support (node 2) to the center of the structure (node 10), which adds up to 9 load cases, as indicated in Figure 5.a. The measurement set N_m=8 (indicated by double arrows) is used here. 2000 samples are generated for both error levels of 4% and 8% by Eq. (16). Mean and COV of the estimations of bending stiffnesses under different load cases and different error levels are summarized in Figure 5.b and Figure 5.c.

When the load is applied at node 2, the bending behavior of elements of EI_1, i.e. elements 1~6, is quite activated. The associated mean for $\widehat{EI}_{1,r}$ is 1.003 (E_{level}=4%) and 1.009 (E_{level}=8%), which is insensitive to errors. However, in the case of EI_3, a higher overestimation can be observed when higher errors exist in the measurements. The associated mean for $\widehat{EI}_{3,r}$ is 1.017 (E_{level}=4%) and 1.069 (E_{level}=8%).

When the load moves from node 2 to node 10, the curvature of the elements of EI_1 decreases while the curvature of the elements of EI_3 increases. Correspondingly, an overestimation of $\widehat{EI}_{1,r}$ arises and escalates while the overestimation of $\widehat{EI}_{3,r}$ becomes less severe. Similar variation is found in the COV of $\widehat{EI}_{1,r}$ and $\widehat{EI}_{3,r}$. In a symmetric load case (V_{10}), the mean of $\widehat{EI}_{1,r}$ and $\widehat{EI}_{3,r}$ are the same, marked by the intersection P_1 and P_2 (Figure 5.b). This is the same case for associated COV, marked by the intersection P_3 and P_4 (Figure 5.c). Note that the bending behavior for elements of EI_2 is quite activated under each load case. When the load moves from node 2 to node 10, the curvature of these elements becomes even higher. As a result, a small but perceptible improvement is seen in both the mean and the COV of $\widehat{EI}_{2,r}$.

The analysis of Figure 5 implies that: (1) In the same load case, the deviation and the dispersion of the estimations are much higher in zones of lower curvature. (2) When the curvature increases due to the change of load case, the deviation and dispersion of the estimations decrease correspondingly.(3) it is advisable to apply different load cases to study different zones of the beam. For instance, to identify EI_1, the location of the load at node 2 is the best choice.

4.5 Example 2: Continuous beam bridge

This section illustrates the application of SSI using compatibility conditions to a 30 m+30 m continuous bridge and the applicability of using different load cases to study different zones of this structure.

The variation of the sectional properties is simulated by different values of the bending stiffnesses in different zones. The FEM for this structure and the structural parameters are depicted in Figure 6.a. It is assumed that $EI_{1,r}=EI_{8,r}=1.5\times10^6$ kN·m^2, $EI_{2,r}=EI_{7,r}=1.8\times10^6$ kN·m^2, $EI_{3,r}=EI_{6,r}=2.1\times10^6$ kN·m^2, $EI_{4,r}=EI_{5,r}=2.5\times10^6$ kN·m^2. In this study, {v_2~v_{12} and v_{14}~v_{24}} are measured and a point load is positioned along the deck to provide different static load cases. For each load case, measurements are generated 2000 times by Eq. (16) using an error level of 4%. The mean and COV of the estimations are summarized in Figures 6.b and 6.c. Due to the symmetry of the structure, only the results for half of the structure is provided.

In Figure 6.b, the bias in the mean of the estimations is generally within 2%. The largest bias is seen in $\widehat{EI}_{3,r}$ and $\widehat{EI}_{4,r}$ with a magnitude of around 5% when the load case is V_5. When the load is applied at zones associated with EI_3 and EI_4, i.e. from V_7 to V_{12}, associated bias decreases greatly, In Figure 6.c, when the load is moved from V_2 to V_{10}, the curvatures of zones related with EI_1 and EI_2 always decrease. Consequently, the COVs for $\widehat{EI}_{1,r}$and $\widehat{EI}_{2,r}$ generally increase. In the case of $\widehat{EI}_{3,r}$ and $\widehat{EI}_{4,r}$, their COVs decrease first due to the increase of curvatures in associated zones. However, when the load is quite close to the middle support, a high proportion of the load is borne by the

middle support and insignificant bending behavior is induced in the structure. As a result, a sharp increase of COV is observed in Figure 6.c when the load cases vary from V_{10} to V_{12}.

Since the mean of the estimations is generally around one, the best load case for a targeted bending stiffness is selected as the load case leading to the lowest dispersion of associated estimations. Figure 6.c shows that the variation of COV largely depends on the load cases. The lowest COVs for EI_1 and EI_2 are 0.044 (V_2) and 0.058 (V_5), respectively. They increases to 0.182 and 0.154, respectively, when the load is positioned at V_{12}. The best load case for estimating EI_3 seems to be V_{11}. However, note that the COV curve for $\widehat{EI}_{6,r}$ is always lower than the COV curve for $\widehat{EI}_{3,r}$ in all load cases. Due to the symmetry of the structure, the estimation of EI_6 using a load in the first span is the same as the estimation of EI_3 using the associated symmetric load in the second span. Hence, the optimal load case for estimating EI_3 is symmetric to the load case having the lowest COV of $\widehat{EI}_{6,r}$ (i.e. V_{10}). Due to the symmetry between V_{10} and V_{16}, the load case V_{16} yields the best estimation of EI_3. The associated COVs for EI_3 are 0.070 (V_{11}) and 0.095 (V_{16}), indicating a decrease of 26.3%. Similarly, the lowest COV of $\widehat{EI}_{5,r}$ occurs at V_9. Concerning the symmetry between EI_4 and EI_5 as well as the symmetry between V_9 and V_{17}, the load case V_{17} yields the best estimation of EI_4. The best mean, COVs and the load locations for $\widehat{EI}_{1,r}$~$\widehat{EI}_{4,r}$ are listed in Table 2. Due to the symmetry, the results for $\widehat{EI}_{5,r}$~$\widehat{EI}_{8,r}$ are not included.

It should be mentioned that, Maxwell-Betti reciprocal theorem can be exploited to reduce the number of sensors while still getting dense measurements[7,36], providing that the response induced by the excitation is still in elastic range. When one sensor is fixed and a point load is positioned at different locations, the readings of the sensor represent the deflections of the structure at the various locations of the load when applying the load at the location of the sensor. This is to say, when the load is positioned at different locations, the placement of one sensor is the same as adding one load case. This can be achieved by positioning a truck with calibrated weight at various locations along the bridges[37]. Hence, in order to get accurate and robust estimations of EI_1~EI_8, it is recommended to place sensors at nodes 2, 5, 16, 17, 9, 10, 21 and 24 together with a load positioned at various locations on the structure.

This example shows the applicability of using different load cases to obtain reliable estimations of the bending stiffnesses for different zones in a continuous beam. The best load case for a targeted bending stiffness is selected as the one leading to the lowest dispersion of associated estimations.

5: Conclusions

This paper proposes a novel approach for identifying compatibility conditions, the relations among displacements, in beam-like structure using observability method. By solving an underdetermined system of equations formulated by compatibility conditions, it is shown that all displacements in a beam-like structure are functions of a subset of these displacements. Then an optimization procedure is introduced to reduce the measurement errors by minimizing the square sum of the proportional deviation of the measured displacements and those compatible displacements. In the numerical simulation, it is shown that when compatibility conditions are not imposed: (1) Regardless of the error level, great bias exists in the estimations though redundant measurements are used. (2) The bias is sensitive to the error levels. (3) Using redundant measurements fails to improve the accuracy of the estimation via SSI by OM. After the imposition of compatibility conditions by optimization, the performance of the proposed method is investigated regarding the number of measurements, error levels and load cases. It is concluded that: (1) The accuracy and robustness of the estimations are significantly improved when compatibility conditions are imposed. (2) The curvature of the zones where parameters are estimated is of vital importance: In the same load case, the deviation and dispersion of the estimations are much higher in zones of lower curvature. Also, the deviation and dispersion of the estimations increase faster with error levels in these zones than in zones of higher curvature. (3) The improvement of the estimation due to the

increase of measurements is more significant in low curvature zone. (4) For zones where curvature is excited, small number of measurements is sufficient to achieve reasonable accuracy. In addition, the deviation in the mean of the estimation is not sensitive to the error levels in these zones. (5) Different load cases can be applied to achieve reliable estimations of parameters for different zones.

The overall performance of the proposed algorithm illustrates its potential application in the SSI for beam-like structures. However, a possible direction of the future research could be the optimal sensor placement for various types of structures and the experimental verification for the proposed method.

Acknowledgement

This work was partially funded by the Spanish Ministry of Economy and Competitiveness and the FEDER fund through the grant project (BIA2013-47290-R) directed by Jose Turmo. It is also to be noted that part of this work was done through a collaborative agreement between Tongji University (China) and Technical University of Catalonia, UPC, BarcelonaTech. This included an exchange of faculty financed by the Chinese government. The financial support from the High End Foreign Experts program (GDW20143100115) from the Chinese government is greatly appreciated. Funding for this research has been provided to Mr. LEI Jun by the Chinese Scholarship Council through its program (No.201506260116) and by the Spanish Ministry of Economy and Competitiveness through its program (BES-2014-07022) for his PhD stays.

Reference

[1] American Society of Civil Engineers, *Structural Identification of Constructed Systems*, American Society of Civil Engineers, Reston, VA **2013**

[2] S. Li, Z. WU, *J. Appl. Mech.*, **2005**, *8*, 943

[3] J.A. Lozano-Galant, M. Nogal, E. Castillo, J. Turmo, *Comput. Civ. Infrastruct. Eng.*, **2013**, *28*, 434

[4] M. Nogal, J.A. Lozano-Galant, J. Turmo, E. Castillo, *Struct. Infrastruct. Eng.*, **2015**, *12*, 1216

[5] M. Sanayei, G. Imbaro, J. McClain, L. Brown, *J. Struct. Eng.*, **1997**, *123*, 792

[6] F. Bakhtiari-Nejad, A. Rahai, A. Esfandiari, *Eng. Struct.*, **2005**, *27*, 1784

[7] Z. Sun, T. Nagayama, Y. Fujino, *J. Civ. Struct. Heal. Monit.*, **2016**, *6*, 255

[8] X. Jiang, H. Adeli, *Int. J. Numer. Methods Eng.*, **2007**, *71*, 606

[9] E.L. Eskew, S. Jang, *Struct. Control Heal. Monit.*, **2017**, *24*, e1899

[10] I. Behmanesh, B. Moaveni, *Struct. Control Heal. Monit.*, **2015**, *22*, 463

[11] E. Habtour, D.P. Cole, J.C. Riddick, V. Weiss, M. Robeson, R. Sridharan, A. Dasgupta, *Struct. Control Heal. Monit.*, **2016**, *23*, 1442

[12] Z. Li, H.S. Park, H. Adeli, *Struct. Des. Tall Spec. Build.*, **2017**, *26*, e1312

[13] J.P. Amezquita-Sanchez, H. Adeli, *Smart Mater. Struct.*, **2015**, *24*, 65034

[14] R. Brincker, C.E. Ventura, *Introduction to operational modal analysis*, John Wiley & Sons, Chichester, UK **2015**

[15] L. Mei, A. Mita, J. Zhou, *Struct. Control Heal. Monit.*, **2016**, *23*, 218

[16] R. Okada, N. Nakata, B.F. SPENCER Jr, K. Kasai, S.B. Kim, *J. Earthq. Eng.*, **2006**, *10*, 97

[17] X. Jiang, S. Mahadevan, H. Adeli, *Struct. Control Heal. Monit.*, **2007**, *14*, 333

[18] G.C. Marano, G. Quaranta, G. Monti, *Comput. Civ. Infrastruct. Eng.*, **2011**, *26*, 92

[19] A.M. Raich, T.R. Liszkai, *Comput. Civ. Infrastruct. Eng.*, **2012**, *27*, 95

[20] Y.-C. Ni, X.-L. Lu, W.-S. Lu, *Struct. Control Heal. Monit.*, **2016**, *23*, 838

[21] J.L. Beck, L.S. Katafygiotis, *J. Eng. Mech.*, **1998**, *124*, 455
[22] H. Sun, R. Betti, *Comput. Civ. Infrastruct. Eng.*, **2015**, *30*, 602
[23] J.L. Beck, S.-K. Au, *J. Eng. Mech.*, **2002**, *128*, 380
[24] F.L. Zhang, H.B. Xiong, W.X. Shi, X. Ou, *Struct. Control Heal. Monit.*, **2016**, *23*, 1366
[25] W.C. Su, C.S. Huang, C.H. Chen, C.Y. Liu, H.C. Huang, Q.T. Le, *Comput. Civ. Infrastruct. Eng.*, **2014**, *29*, 738
[26] E. Castillo, A.J. Conejo, R. Eva Pruneda, C. Solares, *Comput. Oper. Res.*, **2007**, *34*, 1708
[27] S. Díaz, J. González, R. Mínguez, *J. Water Resour. Plan. Manag.*, **2016**, *142*, 4015071
[28] A. Abur, A.G. Exposito, *Power system state estimation: theory and implementation*, CRC press, Boca Raton, FL **2004**
[29] S. Agarwal, P. Kachroo, S. Contreras, *IEEE Trans. Intell. Transp. Syst.*, **2016**, *17*, 1168
[30] E. Castillo, M. Nogal, J.A. Lozano-Galant, J. Turmo, *Math. Probl. Eng.*, **2016**, *2016*, 25
[31] J.A. Lozano-Galant, M. Nogal, I. Paya-Zaforteza, J. Turmo, *Struct. Infrastruct. Eng.*, **2014**, *10*, 1331
[32] J.A. Lozano-Galant, M. Nogal, J. Turmo, E. Castillo, *Comput. Concr.*, **2015**, *15*, 771
[33] M. Sanayei, B. Arya, E.M. Santini, S. Wadia-Fascetti, *Comput. Civ. Infrastruct. Eng.*, **2001**, *16*, 12
[34] M.A.-B. Abdo, *Eng. Struct.*, **2012**, *34*, 124
[35] J. Lei, J.A. Lozano-Galant, M. Nogal, D. Xu, J. Turmo, *Struct. Control Heal. Monit.*, **2016**, doi: 10.1002/stc.1923
[36] C. Wang, C. Huang, C. Chen, *Adv. Adapt. Data Anal.*, **2011**, *3*, 417
[37] E. Bell, P. Lefebvre, M. Sanayei, *J. Struct. Eng.*, **2013**, 1771

Table 1. Mean of the estimations for different bending stiffnesses by SSI by OM without compatibility conditions

Error level	$\widehat{EI}_{1,r}$	$\widehat{EI}_{2,r}$	$\widehat{EI}_{3,r}$
1%	0.85	0.79	0.88
2%	0.76	0.70	0.80
3%	0.73	0.68	0.76
4%	0.72	0.67	0.72
5%	0.72	0.68	0.71
6%	0.74	0.65	0.68
7%	0.70	0.62	0.64
8%	0.70	0.62	0.66

549 Table 2. The best mean, COVs and the associated load cases for the estimations, $\widehat{EI}_{1,r}$~$\widehat{EI}_{4,r}$

	$\widehat{EI}_{1,r}$	$\widehat{EI}_{2,r}$	$\widehat{EI}_{3,r}$	$\widehat{EI}_{4,r}$
Mean	0.996	1.006	0.998	1.005
COV	0.044	0.058	0.070	0.104
Best load case	V_2	V_5	V_{16}	V_{17}

550

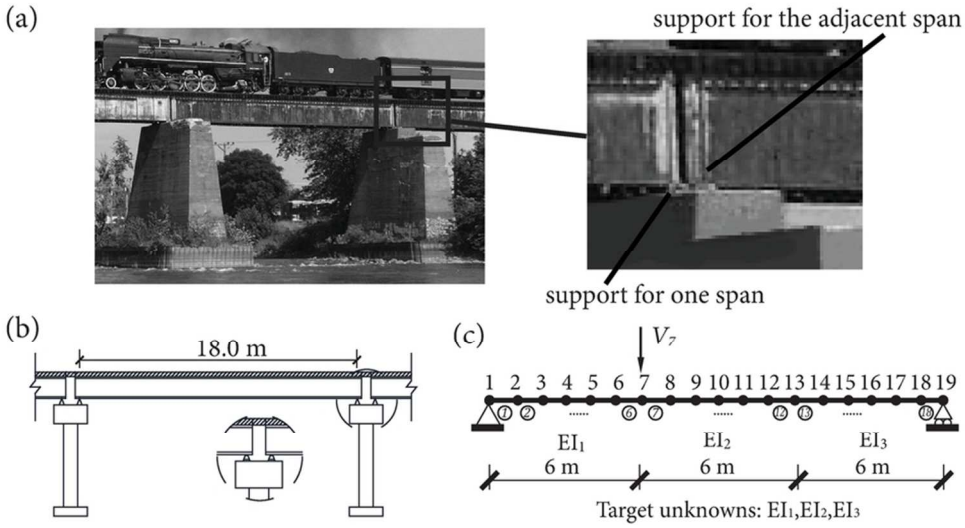

Figure 1. (a) Engineering practice of a multi-span simply supported beam; (b) Elevation of 18 m span of a simply supported bridge; (c) 19-node beam model for the structure in (b).

83x45mm (300 x 300 DPI)

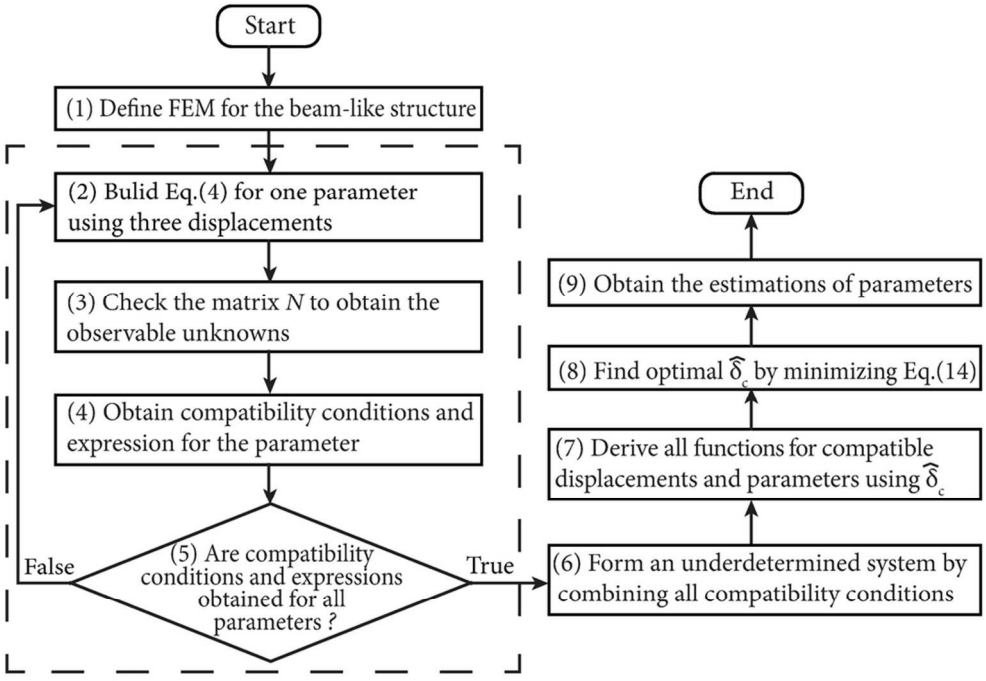

Figure 2. Flowchart for SSI for beam-like structures using compatibility conditions

92x65mm (300 x 300 DPI)

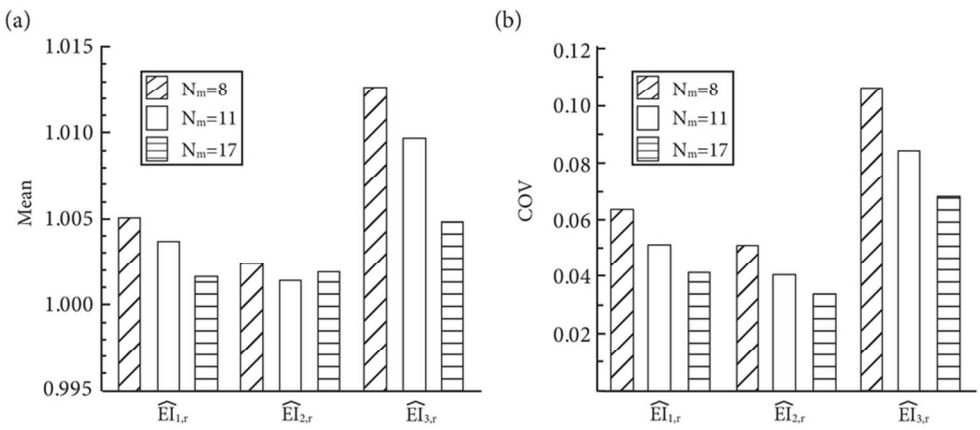

Figure 3. Using N_m=8,11,17 measurements under error level of 4%: (a) Mean of the estimations. (b) The coefficients of variation (COV) of the estimations

84x36mm (300 x 300 DPI)

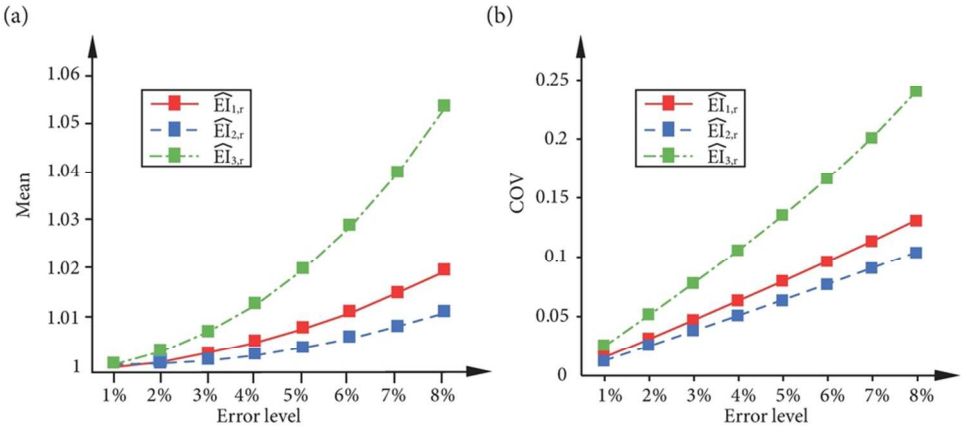

Figure 4. Using N_m=8 measurements under error levels of 1%~8%: (a) Mean of the estimations. (b) The coefficients of variation (COV) of the estimations

86x37mm (300 x 300 DPI)

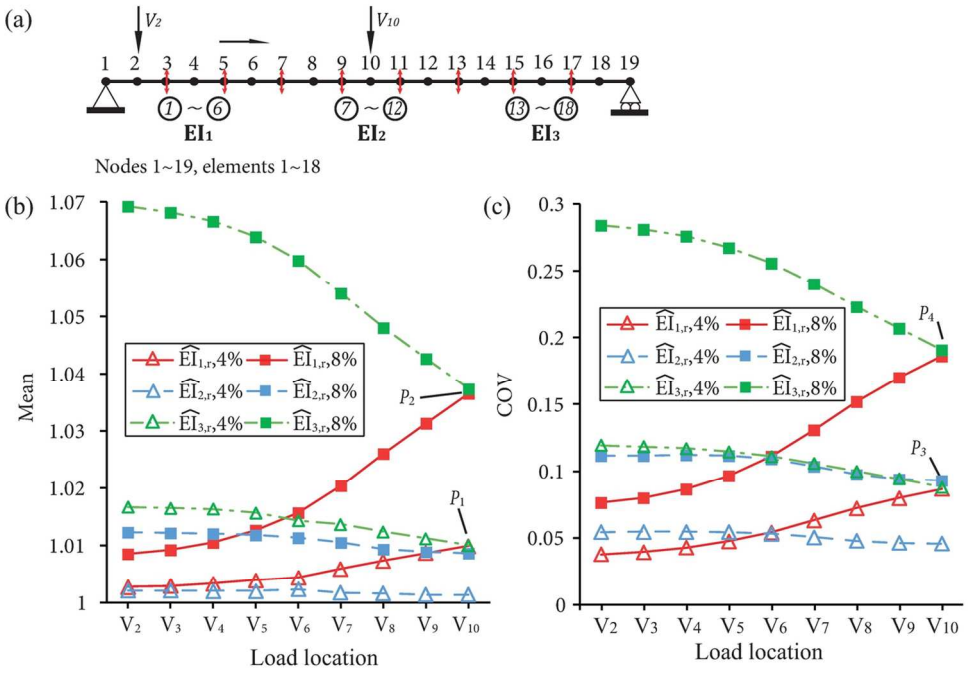

Figure 5. (a) Different load cases (V_2~V_{10}) and measurements (indicated by double arrows); (b) Mean of the estimations under different load cases with Error=4% and 8%; (c) The coefficients of variation (COV) of the estimations under different load cases with Error=4% and 8%;

125x87mm (300 x 300 DPI)

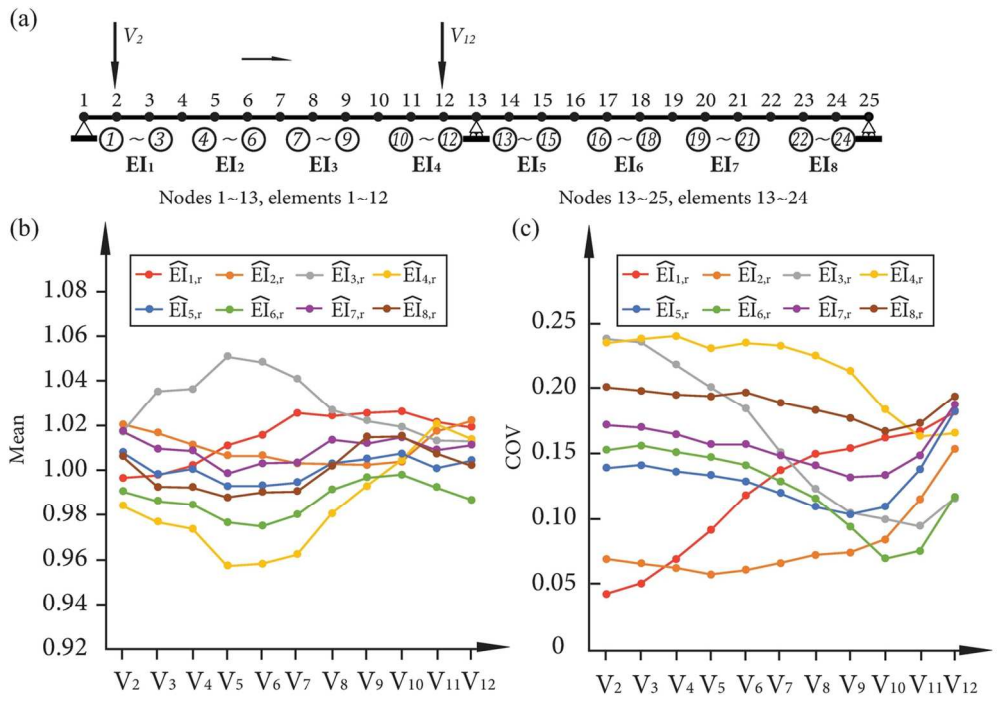

Figure 6. (a) Different load cases (V_2~V_{12}) and measured deflections(v_2~v_{12},v_{14}~v_{24}); (b) Mean of the estimations under different load cases with Error=4%;(c) The coefficients of variation (COV) of the estimations under different load cases with Error=4%

128x91mm (300 x 300 DPI)